ChemistryEurope

ChemistryEurope
Excellence in Chemistry Research Worldwide

RESEARCH ARTICLE OPEN ACCESS

Neutron Crystallography Study of Host–Pathogen Recognition Enhanced by Hydrogen/Deuterium Exchange on Carbohydrates

Theodore Arnaud[1,2] | Chloé Tatol[3] | Juliette M. Devos[4] | Lukas Gajdos[2] | Sébastien Vidal[5] | Marek Korsak[6,7] | Annabelle Varrot[1] | Michaela Wimmerova[6,7] | Sophie Feuillastre[3] | Matthew P. Blakeley[2] | Anne Imberty[1]

[1]CERMAV, Université Grenoble Alpes, CNRS, Grenoble, France | [2]Large Scale Structures Group, Institut Laue-Langevin, Grenoble, France | [3]Service de Chimie Bio-organique et Marquage, DMTS, CEA, Université Paris-Saclay, Gif-sur-Yvette, France | [4]Biology, Deuteration, Chemistry and Soft Matter Group, Institut Laue-Langevin, Grenoble, France | [5]Institut de Chimie des Substances Naturelles, UPR 2301, CNRS, Université Paris-Saclay, Gif-sur-Yvette, France | [6]Central European Institute of Technology, Masaryk University, Brno, Czech Republic | [7]National Centre for Biomolecular Research, Faculty of Science, Masaryk University, Brno, Czech Republic

Correspondence: Sophie Feuillastre (sophie.feuillastre@cea.fr) | Matthew P. Blakeley (blakeleym@ill.fr) | Anne Imberty (anne.imberty@cermav.cnrs.fr)

Received: 27 October 2025 | **Revised:** 22 December 2025 | **Accepted:** 6 January 2026

Keywords: carbohydrates | host–pathogen interaction | isotope labeling | lectin | neutron diffraction

ABSTRACT

Neutron macromolecular crystallography (NMX) is a unique tool for location of hydrogen atoms. Its application is greatly enhanced by the use of deuterium-labeled molecules. Human glycans are the targets of virulence factors from pathogens, such as the soluble lectins from the opportunistic bacterium *Pseudomonas aeruginosa*. Deuterated galactose was obtained by hydrogen isotope exchange and cocrystallized with a fully deuterated bacterial receptor, LecA, a lectin involved in *P. aeruginosa* tissue adhesion and biofilm formation. The structure of the complex determined using neutron diffraction reveals the positions of all hydrogen atoms, as deuterium, highlighting the important role of a charged histidine in the binding site, the bridging by a buried water molecule and the influence of the coordinating calcium ion on the adjacent hydrogen bonds. LecA is a target for pathoblockers and these structural details can assist in the design of glycomimetics for fighting multidrug resistant infections.

1 | Introduction

Hydrogen (^{1}H) atoms are the most abundant constituents of biomolecules, accounting for almost half of the atoms in protein molecules. They are essential for stabilizing biomolecular structures and play crucial roles in the complex energy landscape of proteins [1]. Hydrogen atoms mediate intra- and intermolecular interactions through hydrogen bonds, CH–π or van der Waals interactions. Deuterated biomolecules, in which some, or all hydrogen atoms are replaced by deuterium (^{2}H), are widely used in various domains, notably in drug development [2, 3], mechanistic studies of (bio)chemical processes [4] and smart materials [5, 6]. Deuterated proteins are of particular interest in structural biology, particularly for investigations using NMR [7], neutron diffraction [8] or neutron scattering techniques [9].

Deuterium-labeled small molecules, including carbohydrates, also have wide applications. For instance, labeled carbohydrate analogs are essential tools for the study of biomolecular dynamics (in vivo kinetics) [10, 11], structural elucidation of biomacromolecules [12], study of metabolism [13, 14] and are valuable chiral building blocks [15]. Deuterated carbohydrates have also been used as detergents for studying membrane proteins in small-angle neutron scattering experiments [16]. Since protein–carbohydrate interactions are involved in a wide range of biological processes, neutron crystallography studies of perdeuterated protein–carbohydrate complexes have been performed to

Theodore Arnaud and Chloé Tatol participated equally to the research.

determine the position of hydrogen atoms (as deuterium) in carbohydrate-binding sites. Perdeuterated D-xylulose and D-glucose were used for characterizing the enzyme mechanism in xylose isomerase [17, 18] and more recently, perdeuterated L-fucose was used to reveal the hydrogen bond networks in the binding sites of certain bacterial lectins [19, 20].

While partial deuteration can be obtained via exchange of labile hydrogen atoms of O—H, N—H and S—H bonds by D_2O soaking or vapor diffusion, perdeuteration, i.e., the overall replacement of hydrogen atoms by deuterium atoms, requires stringent methodology. Biotechnology approaches are efficient for the production of recombinant deuterated proteins in bacteria after appropriate accommodation [21]. For other biomolecules that are not directly produced through gene transcription, more complex synthetic strategies are required. In the case of carbohydrates, perdeuterated glucose and mannose were first obtained from algae grown in 99.6% D_2O medium [22, 23], while perdeuterated cellulose and heparosan were produced from bacterial culture [24, 25]. Recently, we glyco-engineered *Escherichia coli* with the introduction of genes coding for GDP-fucose synthesis enzymes, fucosyltransferase and fucosidase, for the production of perdeuterated L-fucose in a bioreactor [26].

Another complementary labeling method is hydrogen isotope exchange (HIE), which has revolutionized the field of labeled compounds, allowing late-stage labeling of a wide-range of organic molecules including drugs and complex biomolecules [27, 28]. However, only a few metal-mediated HIE methods have been implemented and optimized for the labeling of carbohydrates using either Raney Ni in D_2O [29, 30] or a noncommercial source of Ru/C (Scheme 1) [31–33]. When using Raney Ni and D_2O on nonreducing carbohydrates, moderate deuterium atom incorporation was observed at the C2, C3 and C4 positions carrying free hydroxyl groups, while no labeling was observed at carbon atoms C1 and C5. Moreover, the labeling of the C6 position was highly dependent of the activation mode used (see Scheme 1). Nevertheless, this technique has been employed for the deuteration of trehalose, as well as methyl pyranosides derived from D-glucose, D-galactose and D-mannose [34]. Similarly, when using a noncommercial source of Ru/C in D_2O and under an atmosphere of H_2 gas, regio- and stereoselective H-to-D exchanges were observed on various pyranosides with good to quantitative deuterium incorporation on carbon atoms bearing hydroxyl groups. Despite their efficiency in delivering deuterated carbohydrates, both HIE methods suffer from drawbacks and limitations. These include the use of harsh experimental conditions in terms of activation or temperature, necessitating a strict control to prevent degradation or epimerization or the use of a hazardous catalyst (Raney Ni) or of a noncommercially available one (Ru/C from N.E. Chemcat Corporation).

Despite the challenges associated with the different strategies required to label biomolecules, the structural insights provided by deuterated molecules are worth the efforts. Neutron diffraction can precisely locate deuterium atoms and deuterated monosaccharides can be used for mapping these atoms in the binding sites of lectins [35]. These glycan-binding proteins play key roles in self-recognition and infection [36]. Their interaction with glycans is based on a combination of hydrogen-bond networks and hydrophobic contacts, all mediated by hydrogen atoms [37], but structural data obtained through neutron diffraction studies are still very limited [38]. Many pathogenic bacteria use lectins to bind specifically to glycans present on human tissues [39] and our previous neutron structure of LecB lectin from the opportunistic pathogen *Pseudomonas aeruginosa* in complex with L-fucose demonstrated the structural basis of an unusually strong affinity for a monosaccharide [19]. *P. aeruginosa* produces another soluble lectin, LecA, that is specific for galactose and has been identified as a virulence factor [40, 41]. The lectin binds specifically to α-galactoside exposed on glycolipids in lungs or guts, resulting in cell and tissue invasion [42, 43]. As such, high-affinity galactose-derived glycomimetics have been designed as competitors with antibacterial activity, which is of strong interest in the view of multiresistant infection [44–46]. The X-ray crystal structure of LecA in complex with galactose demonstrated the bridging role of a calcium ion with the 3,4-*cis*-hydroxyl groups of galactose [47] and novel noncarbohydrate inhibitors targeting the calcium ions are now being investigated [48].

The study presented here focuses on obtaining deuterated galactose for use in neutron macromolecular crystallography (NMX) studies of LecA, in order to determine the role of hydrogen atoms in the specificity of the protein towards the monosaccharide. Knowledge of these crucial details can ultimately help toward the design of high-affinity inhibitors. The neutron structure of the perdeuterated LecA/Gal complex provides unique information about protonation of amino acids, such as an important histidine residue in the binding site and reveals details of hydrogen bonds close to the calcium ion as well as the role of water molecules.

2 | Results

2.1 | Hydrogen Isotope Exchange and Characterization of Resulting Gal-d_5 and Gal-d_{10}

Methyl α-d-galactopyranoside-2,3,4,6,6′-d_5 (designated as α-OMe-Gal-d_5) has been obtained by optimizing the protocol described by Sawama et al. [33], notably by switching their specific source to a commercially available Ru/C source. Methyl α-d-galactopyranoside and the catalyst were mixed in D_2O and placed

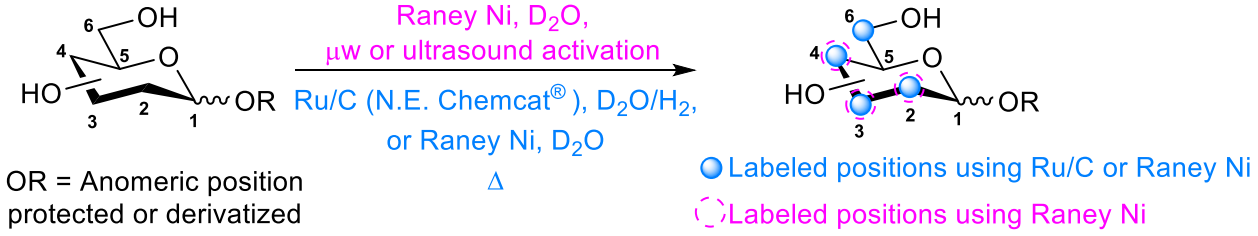

SCHEME 1 | State-of-the-art work using metal-mediated HIE for the labeling of carbohydrates.

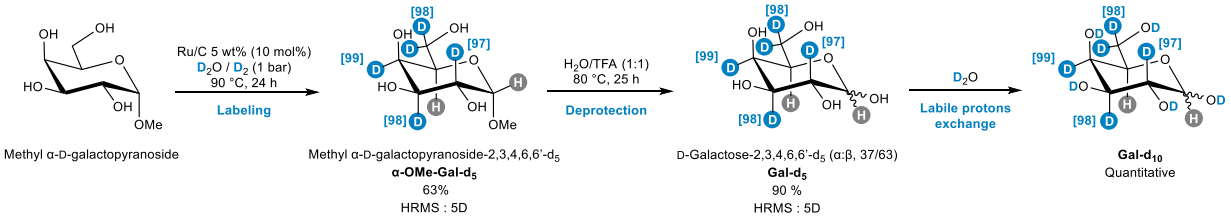

FIGURE 1 | Synthesis of labeled Gal-d_5 and Gal-d_{10} through hydrogen isotope exchange. Isotopic enrichments are indicated between brackets at each labeled position.

under an atmosphere of D_2 gas at 90°C for 24 h, leading to full deuteration of all C—H bonds vicinal to free hydroxyl groups (namely the C2, C3, C4 and C6 positions). D-Galactose-2,3,4,6,6′-d_5 (designated as Gal-d_5) has been obtained thereafter by hydrolysis of the methyl acetal. Soaking of Gal-d_5 in D_2O gave rise to H/D exchange of all O—H bonds to O—D groups, resulting in the Gal-d_{10} compound (Figure 1). All compounds have been analyzed using both NMR spectroscopy (^1H and ^2H) and high-resolution mass spectrometry in order to determine isotopic enrichments at each position, as well as the total deuterium atoms incorporation (Supporting Information).

2.2 | Neutron Structure of the D-LecA/Gal-d_{10} Complex

Recombinant perdeuterated LecA (D-LecA) was produced in *Escherichia coli* high cell-density cultures following adaptation to fully deuterated growth conditions [21] and was purified following established procedures (Supporting Information) [49]. Cocrystals of D-LecA/Gal-d_{10} were obtained in sitting-drop trays using vapor-diffusion combined with regular crystal feeding to produce crystals of sufficient size for NMX experiments [50]. A large cocrystal with volume of ∼0.7 mm^3 (Supporting Information) was used for room-temperature data collection, yielding neutron diffraction to 1.89 Å resolution and X-ray diffraction to 1.45 Å resolution (Table 1). The resulting structure after joint X-ray/neutron refinement displays two tetramers in the asymmetric unit in space group $P2_1$ (i.e., eight chains, labeled A–H) (Supporting Information). The eight chains have very similar structures (C_α RMSD < 0.23 Å) and the overall tetrameric biological assembly is also similar to previously published LecA crystal structures (e.g., PDB:1OKO, Cα RMSD < 0.23 Å) (Figure 2A).

2.3 | Crystallographic Analysis of the Deuteration of Galactose

In all eight chains of the asymmetric unit, clear electron density and neutron scattering-length density (hereafter referred to as neutron density) are observed for the galactose ligand (the average $2mF_o–DF_c$ peak for galactose was above 2.8σ and 1.7σ in the X-ray electron density and neutron density map, respectively). The galactose is in the expected $^4C_1$ chair conformation and presents mostly in the α anomer configuration, which was therefore maintained during the structural refinement procedure. Analysis of the neutron density maps confirmed deuteration on all oxygen atoms and on positions C2, C3, C4 and C6. As expected, the neutron $2mF_o–DF_c$ maps show no peaks indicative of deuterium atoms at carbons C1 and C5, suggesting the presence of hydrogen atoms at these two positions. This is in agreement with the results obtained by NMR and mass spectrometry for the product from HIE synthesis (Figure 2B). Neutron density is observed for deuterium atoms on all hydroxyl groups of Gal-d_{10} allowing for precise visualization of hydrogen bonds (Figures 2B and 3). Only the deuterium on O1 is not clearly localized, likely due to cancelation of the nuclear scattering signal with the hydrogen atom of C1 and perhaps also the local conformational flexibility at this position, as seen when superimposing the galactose residues of the eight chains (Supporting Information).

2.4 | Protonation States of Amino Acids

Inspection of the neutron density maps allows for a detailed analysis of the protonation states of charged amino acids. The imidazole side chain of histidine has a pK_a close to 6 and can exhibit different charged states at physiological pH depending on the local environment. The LecA primary sequence of amino acids contains two histidine residues, His50 and His58. In the LecA/Gal complex (PDB: 1OKO), the NE2 atom of His50 forms a hydrogen bond with O6 of galactose, while the ND1 atom of His58 interacts with a side chain of Asp52, thereby stabilizing the surface loop comprising residues 50–53 involved in the binding site. Analysis of the neutron $2mF_o–DF_c$ density map of the deuterated complex indicates that both histidine residues have their two imidazole nitrogen atoms protonated resulting in a cationic imidazolium (Figure 2C). This observation is consistent with the expected protonation state at the pH of the crystallization solution (pD 5). Further confirmation that both His residues were biprotonated was carried out by performing refinement tests with different protonation states on the two histidine residues of the eight monomers and comparing $2mF_o–DF_c$ and $mF_o–DF_c$ omit neutron density maps (Supporting Information). One aspartic acid residue (Asp100) is involved in both the coordination sphere of calcium and in hydrogen bonding to O4 of galactose. Analysis of the neutron density indicates that this Asp is not protonated.

2.5 | Analysis of the Hydrogen Bond Network in the Binding Site

The binding of galactose in the LecA recognition site results from both the coordination of a calcium ion and an extensive hydrogen bond network (Figure 3). Continuous density is observed for all hydrogen bonds (above 1σ) with clear localization of the

TABLE 1 | Neutron and X-ray data collection and corefinement statistics for the D-LecA/Gal-d_{10} complex.

Data collection	**Neutrons**	**X-rays**
Temperature	291 K	
Crystal size, mm^3	0.74	
Space group	$P2_1$	
a, *b*, *c*, Å	50.80, 106.52, 83.30	
α, β, γ, °	90, 94.63, 90	
Beamline, source	LADI-DALI, ILL	BM07-FIP2, ESRF
Wavelength, Å	2.8–3.8	0.9202
Detector	Image plate	Pilatus 6 M (DECTRIS)
Resolution, Å[a]	45.9–1.9 (2.0–1.9)	44.83–1.49 (1.52–1.49)
No. of unique reflections[a]	50 313 (6352)	142 031 (7042)
R_{merge} (*I*), %[a]	20.6 (42.3)	9.0 (168.8)
R_{pim} (*I*), %[a]	12.5 (20.9)	6.5 (122.7)
Mean $I/\sigma(I)$[a]	6.1 (2.4)	13.0 (0.9)
Completeness, %[a]	72.1 (62.6)	98.8 (99.4)
Multiplicity[a]	3.1 (3.5)	5.4 (5.3)
CC1/2, %	—	99.8 (72.5)
Refinement	**Neutrons**	**X-rays**
Resolution range, Å	45.73–1.89	44.83–1.49
Reflections (used)	50 298	141 805
Reflections (test)	815	2739
R_{work}, %	21.5	15.7
R_{free}, %	27.8	18.5
RMSD in bond lengths, Å	0.014	
RMSD in bond angles, °	1.7	
No. of atoms/Average B factor, $Å^2$		
Protein	14 174/30.6	
Ligand	200/31.7	
Waters	848/41.7	
Ramachandran statistics		
Favored/Allowed/Outliers, %	96.94/93.06/0	
All-atom clash score	5.23	
PDB code	9SQT	

[a]Values for the outer resolution shell are given in parentheses.

deuterium atoms on the hydroxyl groups of the galactose and on asparagine and histidine side chains. Distances and angles characterizing the hydrogen bonds in the binding site are listed in Table 2.

Galactose presents an axial orientation for its O4 hydroxyl group and the hydrogen bond between Gal-O4 and Asp100 is of key importance for the specificity. Gal-O3 accepts a hydrogen bond from the Asn107 side chain and donates one to a water molecule (W2), while Gal-O2 is oriented toward the solvent with hydrogen bonding to water molecule W3. The environment around Gal-O6, is of special interest since this hydroxyl group is accepting a hydrogen bond from protonated His50 and donating one to the side chain oxygen of Gln53. This flexible hydroxymethyl group is therefore trapped in only one conformation, which is unusual for a pyranose hydroxymethyl group. Furthermore, Gal-O6 also accepts a hydrogen bond from a water molecule (W1) that bridges between the galactose and three surrounding amino acids. This water molecule is trapped in a pocket on the protein surface and is conserved in all crystal structures of LecA (Figure 4A). The neutron structure allows the unambiguous determination of its orientation with the water hydrogen atoms directed towards Gal-O6 and the carbonyl group of Pro51 while the water oxygen accepts a hydrogen bond from the main chain nitrogen of Gln53 (Figure 4B).

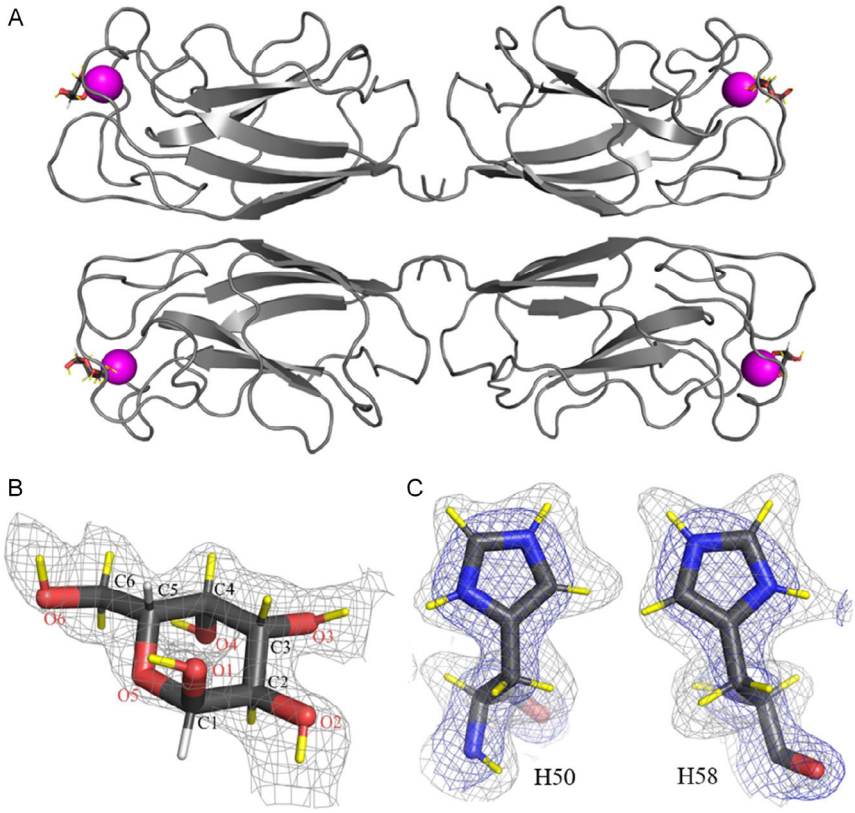

FIGURE 2 | Joint X-ray/neutron crystal structure of D-LecA/Gal-d_{10} complex. (A) Simplified representation of one tetramer (chains A–D) with calcium ions represented as magenta spheres and galactose molecules as sticks. (B) Neutron scattering-length density map shown as gray mesh ($2mF_o–DF_c$ contoured at 1.0σ) around the galactose ligand with deuterium atoms colored yellow and hydrogen atoms (at C1 and C5) colored white. (C) Neutron scattering-length density map in gray ($2mF_o–DF_c$ contoured at 1.0σ) and X-ray electron density map in blue ($2mF_o–DF_c$ contoured at 1.4σ) for charged histidine residues, His50 and His58, of chain A.

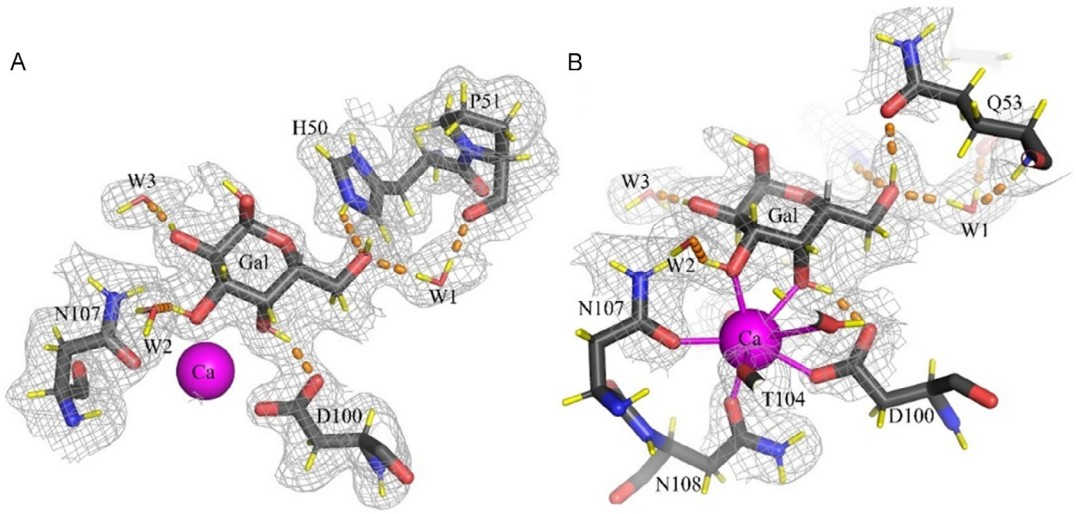

FIGURE 3 | The galactose-binding site in the neutron structure of the D-LecA/Gal-d_{10} complex (chain H). The hydrogen bonds are shown as orange dashed lines. The $2mF_o–DF_c$ neutron density map (gray mesh) is contoured at 0.8σ. (A) Upper view of the binding site with Q53 omitted for clarity. (B) Alternative view including Q53 and displaying the coordination of the calcium ion.

2.6 | Influence of Calcium Ion on Galactose Binding

In the carbohydrate-binding site of LecA, the calcium ion could not be directly observed in the neutron scattering density due to its low neutron scattering cross-section but its position is well defined in the X-ray electron density map. Although calcium coordination in LecA has been previously described [47], our analysis revealed novel insights into the interaction network between galactose and LecA. Specifically, we observed that the orientation of the deuterium atoms on hydroxyl groups

TABLE 2 | Distances and angles for hydrogen bonds involving galactose and a conserved water molecule (W1) with standard deviations calculated across the eight chains of the asymmetric unit.

Donor	Acceptor	Distance, Å	Angle, °
Gal-O2D	W2-O	1.86 ± 0.15	152 ± 15
Gal-O3D	W3-O	1.91 ± 0.25	137 ± 20
Gal-O4D	Asp100-OE1	1.81 ± 0.1	145 ± 15
Gal-O6D	Gln53-OE1	1.99 ± 0.08	138 ± 15
His50-NE2D	Gal-O6	1.91 ± 0.11	146 ± 5
W1-D1	Gal-O6	2.00 ± 0.12	152 ± 12
W1-D2	Pro51-O	1.81 ± 0.06	156 ± 10
Gln53-ND	W1-O	1.96 ± 0.05	160 ± 7

Gal-O3 and Gal-O4 are directed away from the calcium ion. Gal-OD3 participates in a hydrogen bond with water molecule W3, while Gal-OD4 forms a hydrogen bond with the OD1 atom of Asp100 (Figure 3).

Based on previous structures as well as on the distances between galactose oxygens and side chain atoms of Asp100 and Asn107, it was proposed that both Gal-O3 and Gal-O4 establish bifurcated hydrogen bonds with OD1 and ND2 of Asn107 and OD1 and OD2 of Asp100, respectively. The neutron structure indicates a repulsing effect of the calcium ion on the hydrogen atoms, influencing the hydrogen bond network.

2.7 | Influence of His50 Protonation on Affinity

The hydrogen bond observed between His50 and Gal-O6, associated with a conserved orientation of W1 and its hydrogen bond network, depends on the protonation of the NE2 nitrogen atom of His50. At pH higher than 6, His50 is expected to be predominantly neutral, with only one nitrogen atom protonated and the hydrogen bond to Gal-O6 would be either absent or weaker due to neutral charge. This is of importance since physiological pH at the site of infection may vary from 5 to 7.4 depending on the tissue, inflammation state or other aspects [51]. To further investigate the functional role of His50 in the binding site, the interaction of LecA with galactose was analyzed by isothermal titration calorimetry (ITC) at pH values of 5.0 and 7.3. Clear differences were observed with an affinity three times higher at pH 5.0 than at pH 7.3 (Figure 5). The enthalpy of interaction is much stronger at pH 5.0 than at pH 7.3 (−44.1 vs. −34.2 kJ/mol), confirming that hydrogen bonds are more numerous or stronger at acidic pH, when His50 is protonated.

3 | Discussion and Conclusion

A combination of isotope-labeling methods enabled the production of deuterated LecA protein and deuterated galactose. The HIE method developed here is straightforward, easy to implement and provided labeled galactose with maximized isotopic enrichments without degradation or racemization.

Analysis of the neutron structure of D-LecA/Gal-d_{10} complex allowed to identify three key features: (1) the specific orientation of Gal-O3 and Gal-O4 hydroxyl groups induced by the presence of the calcium ion, (2) the critical role of the bridging water molecule in mediating interactions at the Gal-O6 position and (3) the protonation state and involvement of His50 in ligand binding.

The direct involvement of a calcium ion in protein–carbohydrate interfaces has been observed in eight different classes of lectins [37], three of them being from pathogenic microorganisms, i.e., LecA (this study) and LecB [52] from *P. aeruginosa* and epithelial adhesin from *Candida glabrata* [53]. Interestingly, no other metal ion has been observed in such a position. The calcium ion coordination sphere generally involves two adjacent *cis* hydroxyl groups, playing a role in specificity. It can also be involved in pH-dependent affinity of some human C-type lectins [54]. In the neutron structure of D-LecB/Fuc-d_{12} complex, the presence of two calcium ions induces the formation of a low-barrier hydrogen bond between the fucose and the protein, participating in the unusually high affinity of this interaction [19]. In the present structure, analysis of the neutron density demonstrates that the hydrogen atoms on the two coordinating galactose hydroxyl groups are pushed away from the calcium ion, reinforcing the hydrogen bonds between Gal-O4 and Asp100 that are crucial for specificity. This structural knowledge is important for the repurposing of metal-binding active compounds that have been

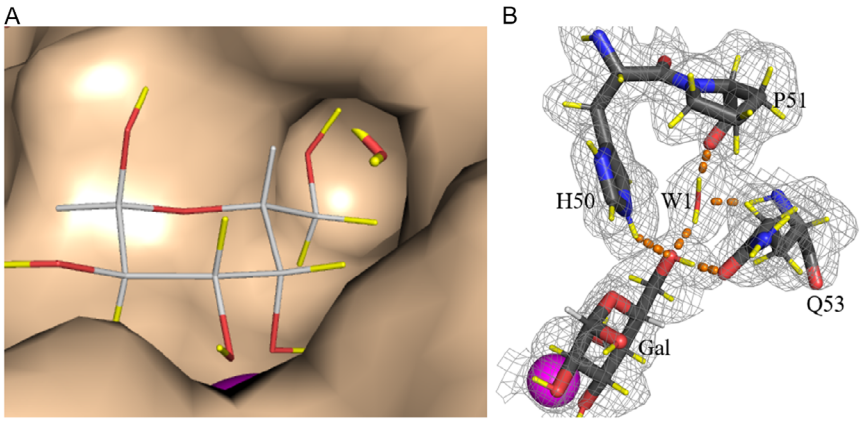

FIGURE 4 | Conserved water molecule W1 in the neutron structure of the D-LecA/Gal-d_{10} complex. (A) Protein surface representation of the binding pocket. (B) Hydrogen-bond network around W1 with the $2mF_o–DF_c$ neutron density map (gray mesh) contoured at 0.8σ.

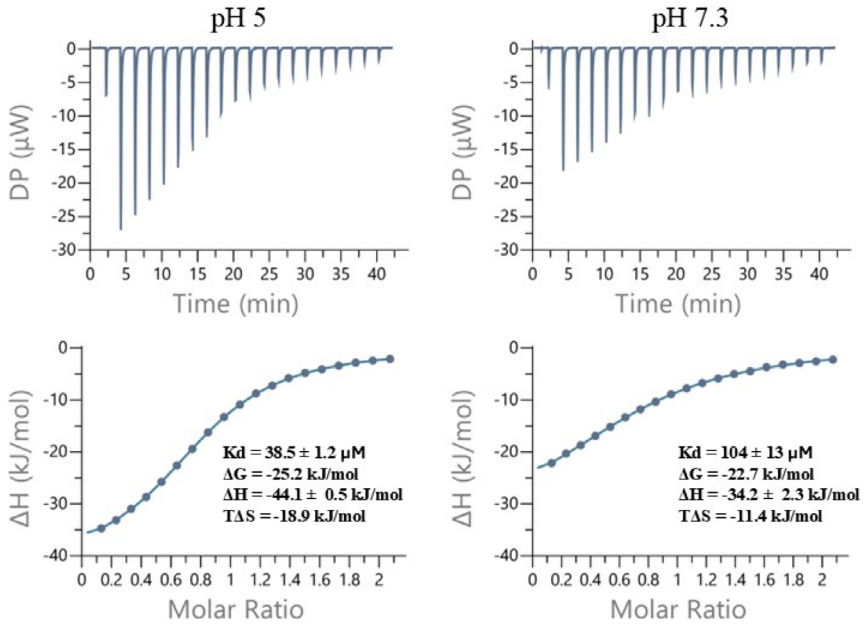

FIGURE 5 | Titration of galactose into LecA solution by ITC at two different pHs. Top: data obtained from 20 automatic injections, 2 µL each, of Gal (3 mM) into the cell containing LecA (0.3 mM). Lower: plot of the total heat released as a function of total ligand concentration for the titration shown above. The solid line represents the best least-squares fit for the obtained data.

recently demonstrated to be efficient noncarbohydrate glycomimetics for inhibition of LecA [48, 55].

Similarly, the importance of a conserved water molecule has been confirmed by the present study. The precise hydrogen bond network involving Gal-O6 and the water molecule trapped in the deep pocket of the binding site was determined. This water molecule (W1) is present in all crystal structures of LecA complexed with galactosides and galactose-derivatives. It has also a crucial role for binding the first noncarbohydrate glycomimetic to be identified, i.e., a cyano-catechol that establishes a contact with W1 through its nitrogen atom [48]. The importance of this water molecule was assessed through a molecular dynamics study that demonstrated its strong stability (occupancy > 90%) [56]. Displacement and replacement of a structural water molecule by a ligand is an efficient strategy to increase the affinity of a ligand via favorable enthalpy of binding [57]. Replacing W1 in LecA through ligand design would appear to be a promising strategy in the quest for high-affinity ligands for LecA, provided that this position can be reached.

The neutron structure of D-LecA/Gal-d_{10} complex was obtained from crystallization performed at acidic pH (pD of 5) and the protonation of the two histidine residues are confirmed by the neutron density map analysis. The thermodynamic contributions measured by ITC correlate the low pH with higher affinity, that is consistent with the occurrence and/or enforcement of the hydrogen bond between His50 and Gal-O6. A more favorable enthalpy of binding with a difference of almost 10 kJ/mol measured between pH 5 and pH 7.3 is only partially counterbalanced by unfavorable entropy. The use of acidic conditions, necessary for obtaining cocrystals, limits the generalization of the observed protonation states and hydrogen bond network. Nevertheless, these conditions may be relevant to the infectious process, since it has been observed that surface liquid in lungs is more acidic in patients with cystic fibrosis [58, 59].

Author Contributions

Theodore Arnaud: investigation (equal), visualization (equal), writing – original draft (equal). **Chloé Tatol**: investigation (equal), visualization (equal), writing – original draft (equal). **Juliette M. Devos**: investigation (equal), methodology (equal), supervision (supporting), writing – original draft (supporting). **Lukas Gajdos**: data curation (equal), investigation (equal), methodology (equal), supervision (supporting), writing – original draft (supporting). **Sébastien Vidal**: conceptualization (equal), funding acquisition (equal), resources (equal), writing – original draft (supporting). **Marek Korsak**: formal analysis (supporting), investigation (supporting). **Annabelle Varrot**: data curation (lead), formal analysis (supporting), investigation (supporting), writing – original draft (supporting). **Michaela Wimmerova**: funding acquisition (supporting), supervision (supporting). **Sophie Feuillastre**: conceptualization (equal), funding acquisition (equal), methodology (equal), supervision (lead), writing – original draft (equal). **Matthew P. Blakeley**: conceptualization (equal), funding acquisition (equal), investigation (equal), methodology (lead), validation (equal), writing – original draft (equal). **Anne Imberty**: conceptualization (lead), funding acquisition (lead), project administration (lead), supervision (lead), writing – original draft (lead).

Acknowledgments

T.A. is supported by both the French National Research Agency in the framework of the France 2030 investment program ANR-22-EXES-0001 and by the Institut Laue Langevin (ILL, Grenoble, France) and C.T. by the French National Research Agency ANR-22-CE07–0017 (Glyco-CD). M.W. and M.K. were supported by the Czech Science Foundation (21-29622S). Glyco@Alps (ANR-15-IDEX-02) is also acknowledged. The authors wish to thank the ILL for provision of beamtime and technical support on the LADI-DALI beamline, for access to the Deuteration Laboratory platform (ILL D-Lab) and for studentship funding to M. K. The authors acknowledge the ESRF (Grenoble, France) for provision of synchrotron radiation beamtime on beamline BM07-FIP2, supported by the French ANR PIA3 (France 2030) EquipEx+ project MAGNIFIX under grant agreement ANR-21-ESRE-0011. The authors thank Sylvain Engilberge for support during the experiment. This work used the

platforms of the Grenoble Instruct-ERIC center (ISBG; UAR 3518 CNRS-CEA-UGA-EMBL) within the Grenoble Partnership for Structural Biology (PSB), supported by FRISBI (ANR-10-INBS-0005-02) and GRAL, financed within the University Grenoble Alpes graduate school CBH-EUR-GS (ANR-17-EURE-0003). The authors thank the SOLEIL synchrotron, Saint Aubin, France for beamtime allocation and the beamline staff of PROXIMA-1 for assistance with data collection.

Funding

This study was supported by Agence Nationale de la Recherche (Grants ANR-22-EXES-0001, ANR-22-CE07-0017, ANR-15-IDEX-02) and Česká vědecká nadace (Grant 21-29622S).

Conflicts of Interest

The authors declare no conflicts of interest.

Data Availability Statement

The data that support the findings of this study are available in the supplementary material of this article.

References

1. N. Engler, A. Ostermann, N. Niimura, and F. G. Parak, "Hydrogen Atoms in Proteins: Positions and Dynamics," *Proceedings of the National Academy of Sciences of the United States of America* 100 (2003): 10243–10248.

2. J. Atzrodt, V. Derdau, W. J. Kerr, and M. Reid, "Deuterium- and Tritium-Labelled Compounds: Applications in the Life Sciences," *Angewandte Chemie International Edition* 57 (2018): 1758–1784.

3. S. Kopf, F. Bourriquen, W. Li, H. Neumann, K. Junge, and M. Beller, "Recent Developments for the Deuterium and Tritium Labeling of Organic Molecules," *Chemical Reviews* 122 (2022): 6634–6718.

4. P. F. Fitzpatrick, "Combining Solvent Isotope Effects with Substrate Isotope Effects in Mechanistic Studies of Alcohol and Amine Oxidation by Enzymes," *Biochimica et Biophysica Acta* 1854 (2015): 1746–1755.

5. J. B. Grimm, L. Xie, J. C. Casler, et al., "A General Method to Improve Fluorophores Using Deuterated Auxochromes," *JACS Au* 1 (2021): 690–696.

6. M. Shao, J. Keum, J. Chen, et al., "The Isotopic Effects of Deuteration on Optoelectronic Properties of Conducting Polymers," *Nature Communications* 5 (2014): 3180.

7. V. Tugarinov, "Indirect use of Deuterium in Solution NMR Studies of Protein Structure and Hydrogen Bonding," *Progress in Nuclear Magnetic Resonance Spectroscopy* 77 (2014): 49–68.

8. M. P. Blakeley and A. D. Podjarny, "Neutron Macromolecular Crystallography," *Emerging Topics in Life Sciences* 2 (2018): 39–55.

9. E. Mahieu and F. Gabel, "Biological Small-Angle Neutron Scattering: Recent Results and Development," *Acta Crystallographica Section D: Structural Biology* 74 (2018):715–726.

10. D. M. Bier, K. J. Arnold, W. R. Sherman, W. H. Holland, W. F. Holmes, and D. M. Kipnis, "In-Vivo Measurement of Glucose and Alanine Metabolism with Stable Isotopic Tracers," *Diabetes* 26 (1977): 1005–1015.

11. D. Indurugalla and A. J. Bennet, "A Kinetic Isotope Effect Study on the Hydrolysis Reactions of Methyl Xylopyranosides and Methyl 5-Thioxylopyranosides: Oxygen versus Sulfur Stabilization of Carbenium Ions," *Journal of the American Chemical Society* 123 (2001): 10889–10898.

12. P. Vallurupalli, L. Scott, M. Hennig, J. R. Williamson, and L. E. Kay, "New RNA Labeling Methods Offer Dramatic Sensitivity Enhancements in 2H NMR Relaxation Spectra," *Journal of the American Chemical Society* 128 (2006): 9346–9347.

13. H. M. De Feyter and R. A. de Graaf, "Deuterium Metabolic Imaging - Back to the Future," *Journal of Magnetic Resonance* 326 (2021): 106932.

14. R. Lowery, M. I. Gibson, R. L. Thompson, and E. Fullam, Deuterated Carbohydrate Probes as 'label-Free' Substrates for Probing Nutrient Uptake in Mycobacteria by Nuclear Reaction Analysis, *Chemical Communications* 51 (2015): 4838–4841.

15. M. Milijkovic, *Carbohydrates: Synthesis, Mechanisms, and Stereoelectronic Effects* (New York: Springer, 2009).

16. S. R. Midtgaard, T. A. Darwish, M. C. Pedersen, et al., "Invisible Detergents for Structure Determination of Membrane Proteins by Small-Angle Neutron Scattering," *The FEBS Journal* 285 (2018): 357–371.

17. A. Y. Kovalevsky, L. Hanson, S. Z. Fisher, et al., "Metal Ion Roles and the Movement of Hydrogen during Reaction Catalyzed by D-Xylose Isomerase: A Joint X-Ray and Neutron Diffraction Study," *Structure* 18 (2010): 688–699.

18. A. Y. Kovalevsky, A. K. Katz, H. L. Carrell, et al., "Hydrogen Location in Stages of an Enzyme-Catalyzed Reaction: Time-of-Flight Neutron Structure of D-Xylose Isomerase with Bound D-Xylulose," *Biochemistry* 47 (2008): 7595–7597.

19. L. Gajdos, M. P. Blakeley, M. Haertlein, V. T. Forsyth, J. M. Devos, and A. Imberty, "Neutron Crystallography Reveals Mechanisms Used by Pseudomonas Aeruginosa for Host-Cell Binding," *Nature Communications* 13 (2022): 194.

20. L. Gajdos, M. P. Blakeley, A. Kumar, et al., "Visualisation of Hydrogen Atoms in a Perdeuterated Lectin-Fucose Complex Reveals Key Details of Protein-Carbohydrate Interactions," *Structure* 29 (2021): 1003–1013.

21. M. Haertlein, M. Moulin, J. M. Devos, V. Laux, O. Dunne, and V. T. Forsyth, "Biomolecular Deuteration for Neutron Structural Biology and Dynamics," *Methods in Enzymology* 566 (2016): 113–157.

22. W. Chorney, N. J. Scully, H. L. Crespi, and J. J. Katz, "The Growth of Algae in Deuterium Oxide," *Biochimica et Biophysica Acta* 37 (1960): 280–287.

23. S. J. Gatley, M. M. Wess, P. L. Govoni, A. Wagner, J. J. Katz, and A. M. Friedman, "Deuterioglucose: Alteration of Biodistribution by an Isotope Effect," *Journal of Nuclear Medicine: Official Publication, Society of Nuclear Medicine* 27 (1986): 388–394.

24. H. O'Neill, R. Shah, B. R. Evans, et al., "Production of Bacterial Cellulose with Controlled Deuterium-Hydrogen Substitution for Neutron Scattering Studies," *Methods in Enzymology* 565 (2015): 123–146.

25. B. F. Cress, U. Bhaskar, D. Vaidyanathan, et al., "Heavy Heparin: A Stable Isotope-Enriched, Chemoenzymatically-Synthesized, Poly-Component Drug," *Angewandte Chemie International Edition* 58 (2019): 5962–5966.

26. L. Gajdos, V. T. Forsyth, M. P. Blakeley, et al., "Production of Perdeuterated Fucose from Glyco-Engineered Bacteria," *Glycobiology* 31 (2021): 151–158.

27. A. Mullard, "FDA Approves First Deuterated Drug," *Nature Reviews Drug Discovery* 16 (2017): 305.

28. C. Schmidt, "First Deuterated Drug Approved," *Nature Biotechnology* 35 (2017): 493–494.

29. S. S. Bokatzian-Johnson, M. L. Maier, R. H. Bell, K. E. Alston, B. Y. Le, and E. A. Cioffi, "Facile C–H Bond Activation for Deuterium and Tritium Labeling of Glycoconjugates Conducted in Ultrasonic and Microwave Fields: A Review," *Journal of Labelled Compounds and Radiopharmaceuticals* 50 (2007): 380–383.

30. J. R. Heys, "Nickel-Catalyzed Hydrogen Isotope Exchange," *Journal of Labelled Compounds and Radiopharmaceuticals* 53 (2010): 716–721.

31. Y. Fujiwara, H. Iwata, Y. Sawama, Y. Monguchi, and H. Sajiki, "Method for Regio-, Chemo- and Stereoselective Deuterium Labeling of Sugars Based on Ruthenium-Catalyzed C—H Bond Activation," *Chemical Communications* 46 (2010):4977–4979.

32. N. Sakurada, D. Sasaki, M. Ono, T. Yamada, T. Ikawa, and H. D. Sajiki, "Development of Site- and Stereoselective Continuous Flow Deuterium Labelling Method for Carbohydrates Using High Dispersion Effect towards Ru/C of Hydrogen Flow," *Reaction Chemistry & Engineering* 10 (2025): 777–781.

33. Y. Sawama, Y. Yabe, H. Iwata, Y. Fujiwara, Y. Monguchi, and H. Sajiki, "Stereo- and Regioselective Direct Multi-Deuterium-Labeling Methods for Sugars," *Chemistry* 18 (2012): 16436–16442.

34. H. J. S. Koch and RS, The Synthesis of Per-*C*-Deuterated D-Glucose," *Carbohydrate Research* 64 (1978): 127–134.

35. J. R. Helliwell, "Relating Protein Crystal Structure to Ligand-Binding Thermodynamics," *Acta Crystallographica* F78 (2022): 403–407.

36. H. Lis and N. Sharon, "Lectins: Carbohydrate-Specific Proteins that Mediate Cellular Recognition," *Chemical Reviews* 98 (1998): 637–674.

37. J. Angulo, J. Zimmer, A. Imberty, and J. Prestergard, *Essentials of Glycobiology* Edited by A. Varki, J. H. Prestegard, R. L. Schnaar et al., (Cold Spring Harbor Laboratory Press, Cold Spring Harbor, 2022):403–418.

38. F. Lisacek, B. Schnider, and A. Imberty, "Tools for Structural Lectinomics: From Structures to Lectomes,"*BBA Advances* 7 (2025): 100154.

39. M. Farez, A. Imberty, and A. Titz, "Bacterial Lectins: Multifunctional Tools in Pathogenesis and Possible Drug Targets," *Trends in Microbiology* 33 (2025): 839–852.

40. O. Bajolet-Laudinat, S. G.-de Bentzmann, J. M. Tournier, et al., "Cytotoxicity of *Pseudomonas aeruginosa* Internal Lectin PA-I to Respiratory Epithelial Cells in Primary Culture," *Infection and Immunity* 62 (1994): 4481–4487.

41. R. S. Laughlin, M. W. Musch, C. J. Hollbrook, F. M. Rocha, E. B. Chang, and J. C. Alverdy, "The Key Role of *Pseudomonas aeruginosa* PA-I Lectin on Experimental Gut-Derived Sepsis," *Annals of Surgery* 232 (2000): 133–142.

42. C. Chemani, A. Imberty, S. de Bentzman, et al., "Role of LecA and LecB Lectins in *Pseudomonas aeruginosa* Induced Lung Injury and Effect of Carbohydrates Ligands," *Infection and Immunity* 77 (2009): 2065–2075.

43. T. Eierhoff, B. Bastian, R. Thuenauer, et al., "A Lipid Zipper Triggers Bacterial Invasion," *Proceedings of the National Academy of Sciences of the United States of America* 111 (2014): 12895–12900.

44. S. Cecioni, A. Imberty, and S. Vidal, "Glycomimetics versus Multivalent Glycoconjugates for the Design of High Affinity Lectin Ligands," *Chemical Reviews* 115 (2015): 525–561.

45. S. Leusmann, P. Menova, E. Shanin, A. Titz, and C. Rademacher, "Glycomimetics for the Inhibition and Modulation of Lectins," *Chemical Society Reviews* 52 (2023): 3663–3740.

46. K. Wojtczak and J. P. Byrne, Structural Considerations for Building Synthetic Glycoconjugates as Inhibitors for *Pseudomonas aeruginosa* Lectins, *ChemMedChem* 17 (2022):e202200081.

47. G. Cioci, E. P. Mitchell, C. Gautier, et al., "Structural Basis of Calcium and Galactose Recognition by the Lectin PA-IL of *Pseudomonas aeruginosa*," *FEBS Letters* 555 (2003): 297–301.

48. S. Kuhaudomlarp, E. Siebs, E. Shanina, et al., "Non-Carbohydrate Glycomimetics as Inhibitors of Calcium(II)-Binding Lectins," *Angewandte Chemie International Edition* 60 (2021): 2–13.

49. B. Blanchard, A. Nurisso, E. Hollville, et al., "Structural Basis of the Preferential Binding for Globo-Series Glycosphingolipids Displayed by *Pseudomonas aeruginosa* Lectin I (PA-IL," *Journal of Molecular Biology* 383 (2008): 837–853.

50. M. Budayova-Spano, K. Koruza, and Z. Fisher, "Large Crystal Growth for Neutron Protein Crystallography," *Methods in Enzymology* 634 (2020): 21–46.

51. I. M. Torres, S. Demirdjian, J. Vargas, B. C. Goodale, and B. Berwin, "Acidosis Increases the Susceptibility of Respiratory Epithelial Cells to *Pseudomonas aeruginosa*-Induced Cytotoxicity," *American Journal of Physiology Lung Cellular and Molecular Physiology* 313 (2017): L126–L137.

52. E. Mitchell, C. Houles, D. Sudakevitz, et al., "Structural Basis for Oligosaccharide-Mediated Adhesion of *Pseudomonas aeruginosa* in the Lungs of Cystic Fibrosis Patients," *Nature Structural Biology* 9 (2002): 918–921.

53. F. S. Ielasi, K. Decanniere, and R. G. Willaert, "The Epithelial Adhesin 1 (Epa1p) from the Human-Pathogenic Yeast *Candida glabrata*: Structural and Functional Study of the Carbohydrate-Binding Domain," *Acta Crystallographica Section D, Biological Crystallography* 68 (2012): 210–217.

54. J. O. Joswig, J. Anders, H. Zhang, C. Rademacher, and B. G. Keller, "The Molecular Basis for the pH-Dependent Calcium Affinity of the Pattern Recognition Receptor Langerin," *The Journal of Biological Chemistry* 296 (2021): 100718.

55. E. Shanina, S. Kuhaudomlarp, E. Siebs, et al., "Targeting Undruggable Carbohydrate Recognition Sites through Focused Fragment Library Design," *Communications Chemistry* 5 (2022): 64.

56. A. Nurisso, B. Blanchard, A. Audfray, et al., "Role of Water Molecules in Structure and Energetics of, *Pseudomonas aeruginosa*, PA-IL Lectin Interacting with Disaccharides," *The Journal of Biological Chemistry* 285 (2010): 20316–20327.

57. P. Matricon, R. R. Suresh, Z. G. Gao, N. Panel, K. A. Jacobson, and J. Carlsson, "Ligand Design by Targeting a Binding Site Water," *Chemical Science* 12 (2020): 960–968.

58. J. Simonin, E. Bille, G. Crambert, et al., "Airway Surface Liquid Acidification Initiates Host Defense Abnormalities in Cystic Fibrosis," *Scientific Reports* 9 (2019): 6516.

59. X. X. Tang, L. S. Ostedgaard, M. J. Hoegger, et al., "Acidic pH Increases Airway Surface Liquid Viscosity in Cystic Fibrosis," *The Journal of Clinical Investigation* 126 (2016): 879–891.

Supporting Information

Additional supporting information can be found online in the Supporting Information section. Material and methods and experimental details for synthesis and characterization, as well as supplemental figures of the crystal structures. **Supporting Scheme S1**: Labeled methyl α-d-galactopyranoside-d_5. **Supporting Scheme S2**: Labeled methyl α-D-galactopyranoside-d_5 with deuteration level on each nonexchangeable position. **Supporting Fig. S1**: ^{1}H NMR spectrum of unlabeled methyl α-D-galactopyranoside. **Supporting Fig. S2**: ^{1}H NMR spectrum of labeled methyl 2,3,4,6,6′-pentadeuterio-α-D-galactopyranoside. **Supporting Fig. S3**: ^{2}H-{^{1}H} NMR spectrum of methyl 2,3,4,6,6′-pentadeuterio-α-D-galactopyranoside. **Supporting Fig. S4**: ^{13}C-{^{1}H} NMR spectrum of methyl 2,3,4,6,6′-pentadeuterio-α-D-galactopyranoside. **Supporting Fig. S5**: HRMS spectrum and data of methyl α-D-galactopyranoside-d_5. **Supporting Fig. S6**: ^{1}H NMR spectrum of 2,3,4,6,6′-pentadeuterio-α-D-galactose. **Supporting Fig. S7**: ^{2}H-{^{1}H} NMR spectrum of 2,3,4,6,6′-pentadeuterio-α-D-galactose. **Supporting Fig. S8**: ^{13}C-{^{1}H} NMR spectrum of 2,3,4,6,6′-pentadeuterio-α-D-galactose. **Supporting Fig. S9**: HRMS spectrum and data of 2,3,4,6,6′-pentadeuterio-α-D-galactose. **Supporting Fig. S10**: SDS-PAGE of perdeuterated LecA during purification. Lanes 6 to 14 show samples taken from various fraction along the main elution peak. **Supporting Fig. S11**: MS showing correct deuteration level of D-LecA. **Supporting Fig. S12**: Crystals of D-LecA/Gal-d_{10} complex used for neutron and X-ray data collection. A: Crystal after initial vapor diffusion phase. B: Crystal from panel A after feeding processes. **Supporting Fig. S13**: Crystal structure (PDB: 9SQT): Two tetramers of D-LecA complexed with Gal-d_{10} (sticks) and calcium in (purple sphere) in the asymmetric unit. **Supporting Fig. S14**: Superimposition of the 8 Gal-d_{10} ligands from the different chains. **Supporting Fig. S15**: Histidine protonation analysis during refinement process. The neutron

$2mF_o$-DF_c density map is shown as gray mesh and contoured at 1σ. The neutron mF_o–DF_c difference density map is shown as mesh contoured at 3σ with positive density in green and negative density in red. All histidines are from Chain C. (A) His50 as unprotonated histidine, (B) His50 as biprotonated, (C) His58 as unprotonated and (D) His58 as biprotonated. **Supporting Fig. S16**: X-ray and neutron densities superimposed at the binding site. The $2mF_o$-DF_c neutron density (gray mesh) and electron density (blue mesh) map is contoured at 0.8σ and 1.5σ, respectively. Calcium ions are shown as purple sphere, W1 and W3 are highly ordered water molecules, Gal-d_{10} is shown in the center of the panels as sticks with important D-LecA residues around, dashed lines are picturing hydrogen bonding distances. (A) Binding site without Gln53. (B) Full binding site representation.